Supplementary Data

Interaction of human telomeric DNA with *N*-methyl mesoporphyrin IX, NMM

John M. Nicoludis[1], Steven P. Barrett[1], Jean-Louis Mergny[2,3], and Liliya A. Yatsunyk[1,*]

[1]Department of Chemistry and Biochemistry, Swarthmore College, 500 College Ave., Swarthmore, PA 190813; [2]Univ. Bordeaux, ARNA Laboratory, IECB, F-33000 Bordeaux, France; [3]INSERM, U869, ARNA Laboratory, European Institute of Chemistry and Biology, 2 rue Robert Escarpit, F-33000 Pessac, France.

Aggregation studies for NMM and NMP

Aggregation state of NMM and NMP was tested by UV-vis absorbance spectroscopy in dilution experiments aimed at determining whether solutions of NMM and NMP adhere to the linear relationship of Beer's law. Ten 1 mL samples with concentrations 1 - 10 μM and ten samples with concentration 14 - 50 μM were prepared in 1 cm methacrylate cuvettes and 2 mm quartz cuvettes, respectively, and their UV-vis spectra were collected. All wavelength scans were baseline corrected. While the concentration of NMM was determined based on reported extinction coefficient, the NMP sample was prepared using analytical techniques and its extinction coefficient in water was determined from the linear dependence of absorbance *vs* concentration (**Figure S1**) to be 1.0×10^5 $M^{-1}cm^{-1}$.

Singular Value Decomposition (SVD) analysis

CD and UV-vis titration data were converted to a matrix M in which each column contains the spectroscopic signal after each addition of NMM and each row corresponds to the wavelengths of the spectra. Matrix M was imported into MATLAB (the Mathworks, Inc., Natick, MA) and decomposed using the SVD method to produce the matrices *U*, *S* and *V* such that: $M = USV^t$ (84), (where *t* stands for transposed). The singular values were converted into relative variance using the following equation: $RV_i = S_i^2 / \Sigma(S_i^2)$ (56). Relative variance can be used to determine the number of significant spectral species. Autocorrelation of *U* and *V* can also aid in determining the number of components present. The first order autocorrelation function is defined as $C(X_i) = \Sigma(X_{j,i})(X_{j+1,i})$ where X is either *U* or *V* (84),

and determines the amount of signal-to-noise of a basis spectrum (U) or amplitude vector (V). Autocorrelation values ≥0.8 are accepted as being significant (84,85)

FRET melting assay

FRET melting assay has a distinct advantage over UV-vis or CD melting, requiring small amounts of DNA and ligands due to its high sensitivity. Experiments could be performed in a 96 well plate format using a RT-PCR instrument allowing for simultaneous testing of a variety of conditions. In addition, FRET provides a unique opportunity to design competition experiments where GQ stability could be determined in the presence of large amount of unlabeled competitor.

The fluorescently-labeled oligonucleotides 5′-6-FAM-GGG(TTAGGG)$_3$-Dabcyl-3′ (F21D) and 5′-6-FAM-G$_3$(TGTGGG)$_3$-Dabcyl-3′ (FGD), were purchased from IDT (Coralville, IA), dissolved in water to a concentration of 0.1 mM and stored at -80 °C. The values of extinction coefficients for FGD and F21D were determined using a nearest neighbor approximation (53) taking into account the absorbance of the fluorescent dyes (data provided by the manufacturer). FGD and F21D were annealed at 10 μM in an appropriate buffer (5K or 50Na), mixed with varying amounts of porphyrins and equilibrated at 30 °C for at least 30 hours prior to collecting melting profiles. Final concentration of oligonucleotides was 0.2 μM and porphyrin 0.4 – 4 μM in 50 μl reactions. The fluorescence of 6-FAM dye was measured at 519 when excited at 496 nm on an MJ research DNA Engine Real-Time PCR machine. For competition experiments, unlabelled double-stranded DNA (ds26 or CT) or parallel GQ DNA (G5 or G8) was included at 4.8, 16, 32 and 96 μM (24, 80, 160 and 480 equivalents relative to fluorescent oligonucleotide) together with 0.2 μM FGD or F21D and 1.6 μM NMM or NMP. Control experiments included buffer alone; F21D or FGD alone; F21D or FGD with 1.6 μM porphyrins; and F21D or FGD with 16 μM competitor. Melting protocol consisted of three steps: 1) incubation at 15 °C for 5 minutes; 2) temperature increase in the stepwise manner from 15.0 to 95.0 °C at 1°C min^{-1} rate, reading fluorescence every 1.0 °C; 3) cooling from 95.0 to 15.0 °C at a rate of 1 °C min^{-1} and recording the fluorescence every 1.0 °C. Each set of experiments included duplicate samples. The melting curves were normalized between 0 and 1 using the equation: $Y' = \frac{Y - Y_{\min}}{Y_{\max} - Y_{\min}}$, where Y is the fluorescence signal. The normalization was necessary so that the data for the duplicate experiments could be averaged correctly. To determine melting temperatures, $T_{1/2}$, the derivatives of the averaged melting curves were calculated, and the peaks were fit using a Lorentz single or multiple peak fit function.

Preparation of competitors for FRET studies

Parallel stranded quadruplexes, $[dTG_5T]_4$ (G5) and $[dTG_8T]_4$ (G8). GQ competitors were dissolved in 95 mM LiCl, 10 mM LiCac, pH 7.2 buffer to a concentration of ~2 mM (per strand). It is important that at this point the buffer contains no potassium ions. Samples were annealed at 90 °C for 10 min and cooled slowly to 75 °C at which point K^+ concentration was brought up to 5 mM. Samples further cooled to ambient temperature over 3 hour period and stored at 4 °C for one week to allow complete equilibration.

Duplex competitors, CT and ds26. Dry sample of CT DNA was dissolved in 10 mM LiCac, 1mM Na_2EDTA to a concentration of ~1mM (in base pair) and placed on nutator for 1 week at 4 °C. Before use sample was spun extensively to remove insoluble components and transferred to a clean eppendorf tube. Dry ds26 oligonucleotide was diluted in 5K buffer to a final concentration of ~1mM (per strand), annealed at 90 °C for 10 min, and cooled slowly to ambient temperature over three hours. This sample was stored at 4 °C for 1 week to allow complete equilibration.

Before use, concentration of all stocks was verified via UV-vis spectroscopy using extinction coefficients found in **Table S1** and is reported per strand in all cases but CT DNA for which it is reported per base pair and G5 and G8 for which it is reported per quadruplex. The folding of all competitors was checked by CD spectroscopy and compared to our previous data or to the literature. All the competitors were stored at 4°C for 4-6 weeks, except for CT DNA which was stored for up to 8 weeks.

Determination of selectivity ratios in FRET competition experiments

Competition with duplex DNA, CT and ds26. Selectivity ratio in this case cannot be determine accurately as no decrease in stabilization temperature was observed even at the highest amount of competitor, 480 eq with respect to labeled DNA. Therefore, the lower limit of selectivity ratio was assigned to the excess of competitor, 480.

Competition with G5 and G8. In order to assign numerical values to the selectivity of NMM and NMP for F21D (or FGD) *vs* G5 or G8, it was assumed that the excess of competitor required for a 50% reduction in $\Delta T_{1/2}$ is roughly proportional to the selectivity ratio (assuming identical number of binding sites for each GQ). With this in hand, the selectivity ratio was estimated to be for F21D 25 (meaning that NMM is 25 times more selective for F21D as compared to G5), 20, 9 and 6 for NMM+G5, NMM+G8,

NMP+G5, NMP+G8, respectively; and for FGD 47, 42, 25, and 17 for NMM+G5, NMM+G8, NMP+G5, NMP+G8, respectively in 5K buffer. In general, while stabilizing temperatures for F21D are higher (see **Table 2**), the selectivity ratios for this oligonucleotide are lower by a factor of 2 as compared to FGD, indicating possible higher affinity of NMM and NMP for the latter oligonucleotide. Now, when G5 and G8 are compared, the selectivity ratios are virtually the same, if a little lower for G8 (this could be due to the larger size of this quadruplex and therefore higher ability of nonspecific binding). In terms of selectivity we can place the quadruplexes in the following order FGD (5K) > F21D (5K) > G8 (5K) ≈ G5 (5K) >> F21D (50Na).

Potassium titration of Tel22:NMM 1:2 mixture monitored by CD

A large batch of 5 μM Tel22 was prepared with 10 μM NMM in 10 mM lithium cacodylate, pH 7.2. It was split into ten samples, which were assembled with increasing concentrations of KCl. Constant ionic strength was maintained at 150 mM by complementary addition of 3 M LiCl. Two additional samples were prepared with 200 and 300 mM KCl, whose resulting ionic strength was ~210 and ~310 mM respectively. Samples were annealed and then diluted to final concentrations of 2.5 μM for Tel22 and 5 μM for NMM. Samples were incubated for >30 h at 30 °C and CD spectra were collected several times throughout this period to assure that complete equilibrium was achieved. A control experiment was performed, where Tel22 was annealed and subsequently incubated at 30 °C with 300 mM KCl but without any NMM. In order to determine the apparent affinity constant (K_a) and stoichiometry (n) for K^+ binding, the normalized CD signal at 264 was fitted to the classical Hill equation.

Potassium binding parameters for Tel22 alone determined by the Chaires group from K^+-induced changes in UV-vis titrations were $n = 1.51 \pm 0.03$ and $K_a = 1.96\times10^3$ (86). A more recent study from the same group, where K^+ binding was measured directly using fluorescent indicator, finds $n = 3$ and $K_a = 5.13\times10^6$ for Tel22 in the presence of 5 mM K^+, condition identical to ours (61). While it seems that Tel22 K^+ binding constant in the absence of NNM is much higher, the comparison is only possible when n is the same in all cases. When all binding constants are recalculated per binding site, the numbers, in fact, are rather similar: $K_a = 320$ M^{-1} for Tel22-NMM, $K_a = 151$ M^{-1} (86) or 172 M^{-1} (61) for Tel22 alone. Our data suggest a lower K^+ stoichiometry (1 vs. 2 or 3) for Tel22 in the presence of NMM, indicating that NMM alters the GQ structure of Tel22 to the new fold that require only one K^+ ion. It is also conceivable, that since our experimental setup and data treatment resemble closely those from reference (86) where $n = 1.5$, the observed stoichiometry in our work is not all that different, $n = 1.1$.

Tables S1

Table S1. Molecules used in this work and their extinction coefficients. Note, all porphyrin extinction coefficients refer to aqueous solutions, unless otherwise noted; all DNA extinction coefficients are reported for 260 nm and per strand, unless otherwise noted.

Abbreviation	**Full name or sequence**	**$\Delta\varepsilon$, M^{-1} cm^{-1}**
NMM	*N*-methyl mesoporphyrin IX	145,000 at 379 nm (45)
NMP	*N*-methyl protoporphyrin IX	100,000 at 383 nm (determined in this work)
MIX	mesoporphyrin IX dihydrochloride	150,000 at 401 nm
PIX	protoporphyrin IX	170,000 at 408 nm in DMSO (87)
TMPyP4	5,10,15,20–tetrakis(*N*-methyl-4-pyridyl) porphyrins	226,000 at 422 nm (71)
Tel22	d[$AG_3(TTAG_3)_3$]	228,500
T_6Tel22	d[$T_6AG_3(TTAG_3)_3$]	277,000
Tel22T_6	d[$AG_3(TTAG_3)_3T_6$]	277,500
ATel26	d[$A_3G_3(TTAG_3)_3AA$]	278,200
GTel26	d[$GG(ATTG_3)_4$]	260,400
F21D	5′-6-FAM-$G_3(TTAG_3)_3$-Dabcyl-3′	247,600
FGD	5′-6-FAM-$G_3(TGTG_3)_3$-Dabcyl-3′	233,100
CT	Genomic calf thymus DNA	12,200 (per base pair)
ds26	5′-CAATCGGATCGAATTCGATCCGATTG-3′	253,200
G5	$[dTG_5T]_4$	67,900
G8	$[d(TG_8T]_4$	98,200
THM	GGGTTGGGTTGGGTTGGG	173,000
26TelG4	AGGGGTTAGGGGTTAGGGGTTAGGGG	268,900
G4TERT	AGGGGAGGGGCTGGGAGGGC	202,900

Bcl-2	GGGCGCGGGAGGGAATTGGGCGGG	237,400
HIF-1α	GGGAGGGAGGGAAGGAGGGAGGGAGGGA	308,300
TBA	GGTTGGTGTGGTTGG	143,300
cKit1	GGGAGGGCGCTGGGAGGAGGG	213,200
cKit2	GGGCGGGCGCGAGGGAGGGG	199,100
VEGF	GGGAGGGTTGGGGTGGG	171,400
cMyc	TGAGGGTGGGTAGGGTGGGTAA	228,700

.

Table S2

Table S2. UV-vis data for NMM annealed in the presence of a variety of GQ-forming sequences. Red-shifts were found by annealing sequences in 5K buffer at a 13-fold excess compared to NMM and subtracting the maximum wavelength of absorbance of NMM alone from the maximum wavelength of absorbance of NMM in the presence of the GQ DNAs. Percent hypochromicity is defined as:

$$\%H = \frac{abs(NMM_{free}^{379nm}) - abs(NMM_{bound}^{\lambda max})}{abs(NMM_{free}^{379nm})} \times 100\%$$

The %H values are our best estimates. NMM adsorbs appreciably to the plastics of the methyl methacrylate cuvettes during prolonged incubations. Therefore values reported carry significant error, in some cases as large as 10%. 4-6 data sets were collected and averaged.

Name	Sequence	Red-shift (nm)	%H
Tel22, 5K	AGGGTTAGGGTTAGGGTTAGGG	19.3 ± 0.4	-3
Tel22, 50Na	AGGGTTAGGGTTAGGGTTAGGG	0.0 ± 0.2	19
26TelG4	AGGGGTTAGGGGTTAGGGGTTAGGGG	18 ± 1	-1
26TelG4, 50Na	AGGGGTTAGGGGTTAGGGGTTAGGGG	19.5	12
Bcl-2	GGGCGCGGGAGGGAATTGGCGGGG	17.2 ± 0.3	-11
cKit1	GGGAGGGCGCTGGGAGGAGGG	18.6 ± 0.9	-5
cKit2	GGGCGGGCGCGAGGGAGGGG	19.2 ± 0.4	-4
cMyc	TGAGGGTGGGTAGGGTGGGTAA	20. ± 1	-1
G4TERT	AGGGGAGGGGCTGGGAGGGC	17.7 ± 0.3	-17
HIF-1α	GGGAGGGAGGGAAGGAGGGAGGGAGGG	18.5 ± 0.7	-4
TBA	GGTTGGTGTGGTTGG	19.5 ± 0.5	13
THM	GGGTTGGGTTGGGTTGGG	17.3 ± 0.9	-12
VEGF	GGGAGGGTTGGGGTGGG	17.3 ± 0.8	-21
G8	TGGGGGGGGT	17.8 ± 0.4	-7
G5	TGGGGGT	17.3 ± 0.4	-13
G8, 50Na	TGGGGGGGGT	18.0	n/d
G5, 50Na	TGGGGGT	18.0	n/d

n/d – not determined

Figure S1

Figure S1. Results of aggregation study for (**A**) NMM and (**B**) NMP. Linear relationships in both cases indicate no aggregation. For NMP extinction coefficient, ε, at 383 nm in water was determined to be 1.0×10^5 $M^{-1}cm^{-1}$ from the slope of the line.

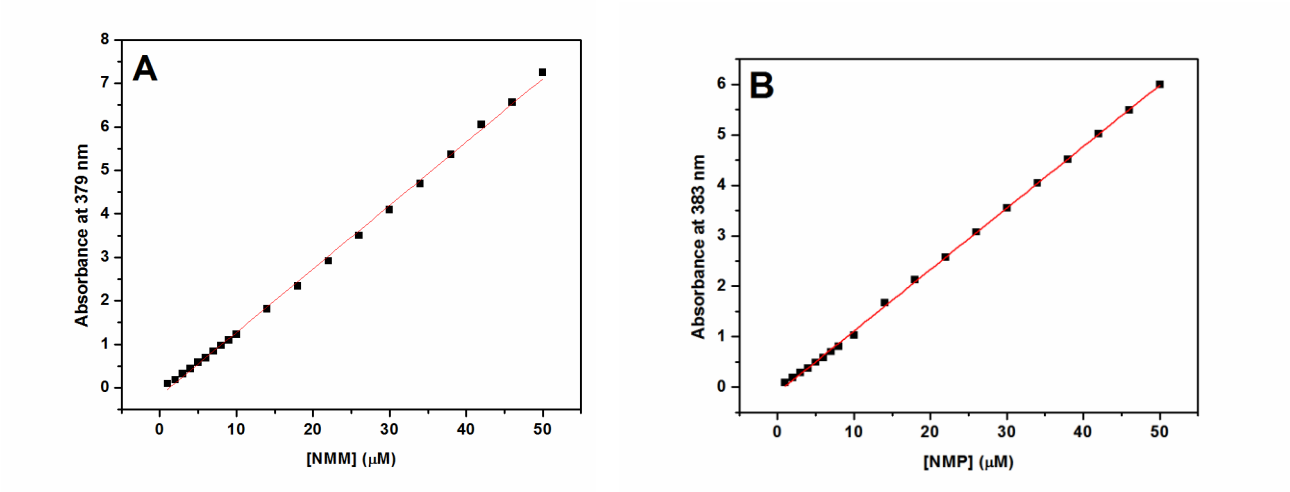

Figure S2.

Figure S2. (**A**) CD spectra of 2.7 μM Tel22 in 5K, 50Na, and 100Li buffers at 25 °C. (**B**) CD spectra of 2.5 μM Tel22 annealed in the presence of 5.0 μM NMP and (**C**) TMPyP4 in 5K buffer.

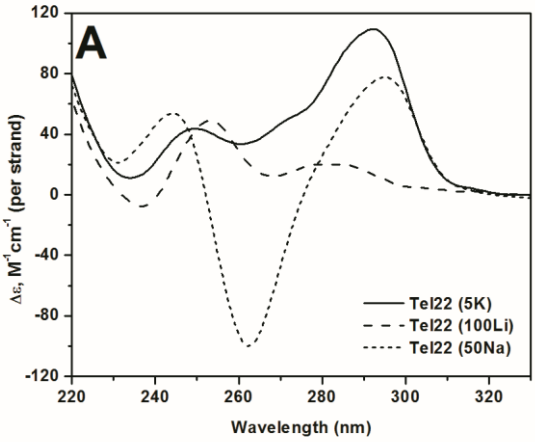

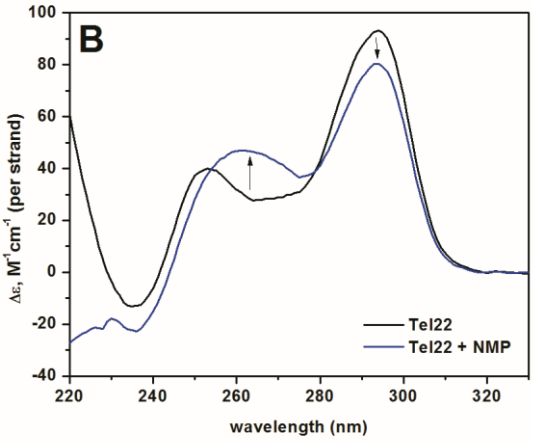

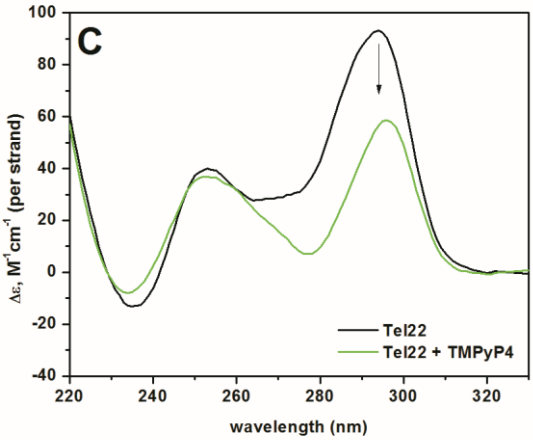

Figure S3

Figure S3. Annealing study of telomeric GQ-forming sequences in the presence of NMM in 5K buffer. Samples of 2.5 μM (**A**) Tel22T_6, (**B**) dA_3G_3($TTAG_3$)$_3$AA, (**C**) dGG($ATTG_3$)$_4$, (**D**) T_6Tel22, and 4 μM **(E)** dAG_4($TTAG_4$)$_3$ (26TelG4) were annealed with 2eq of NMM. The solid line represents the CD spectrum of oligonucleotides annealed alone; the dotted line is the spectrum of oligonucleotides annealed in the presence of NMM; and the dashed line is the spectrum of oligonucleotides to which NMM was added after annealing and cooling to 30 °C. All samples were incubated for >12 h at 30 °C, and the CD spectra were collected at 25 °C.

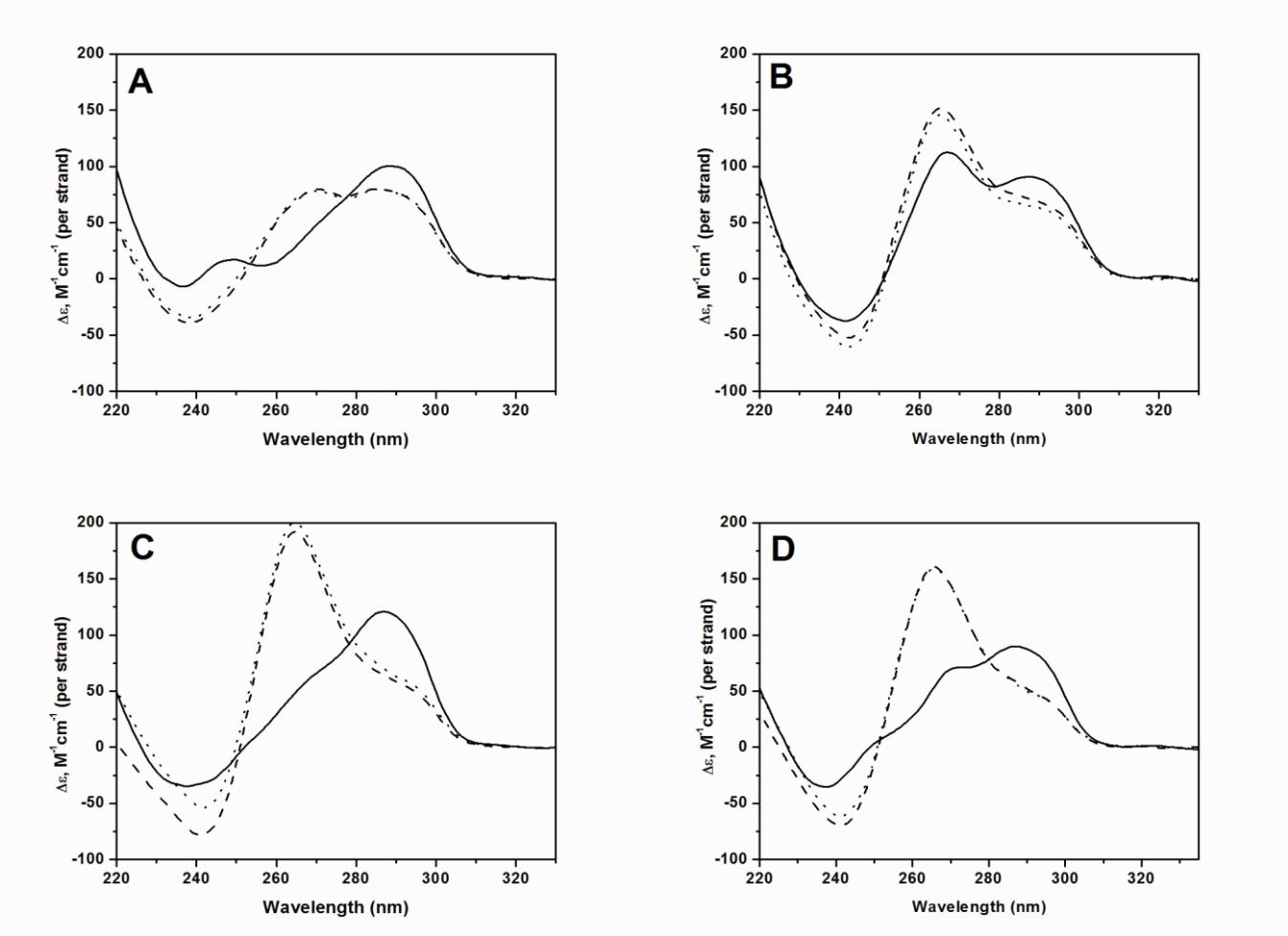

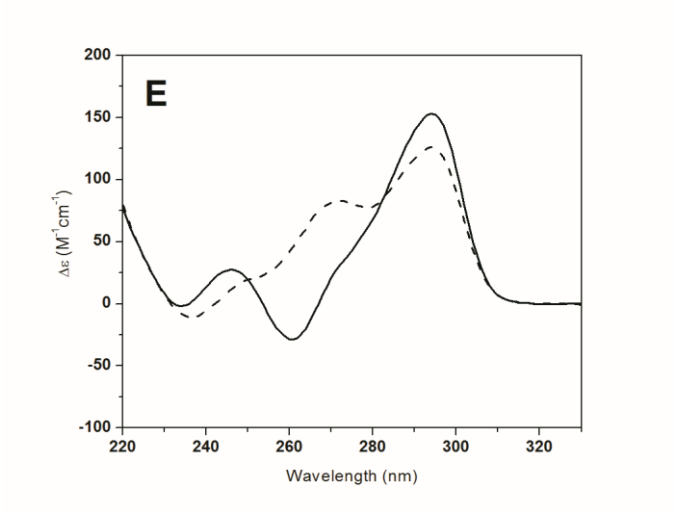
E
200
150
100
50
0
-50
-100
220
240
260
280
300
320
Δε (M⁻¹cm⁻¹)
Wavelength (nm)

Figure S4

Figure S4. (A) CD annealing study of GQ-forming sequences (other than human telomeric DNA) in the presence of NMM in 5K buffer. Samples of 4-6 μM DNA were annealed at 90 °C for 10 min without (solid lines) or with (dotted lines) 2 equivalents of NMM, cooled to 30 °C slowly and stored at 30 °C for >12 h. (**B)** UV-vis spectra of NMM (2.3 μM) without (black) and with ~20 eq. of representative non-telomeric GQ-forming sequences. Sequences of oligonucleotides can be found in **Table S1.** (**C**) Negative induced CD signal in the visible region observed for mixtures of NMM with cMyc, VEGF, and HIF-1α after prolonged incubation. Note, no induced signal is seen for NMM/TBA in 5K, NMM/Tel22 in 50Na. Other sequences that display induced signal in the presence of NMM include 26TelG4, Bcl-2, cKit1, cKit2, G4TERT, and THM.

(A)

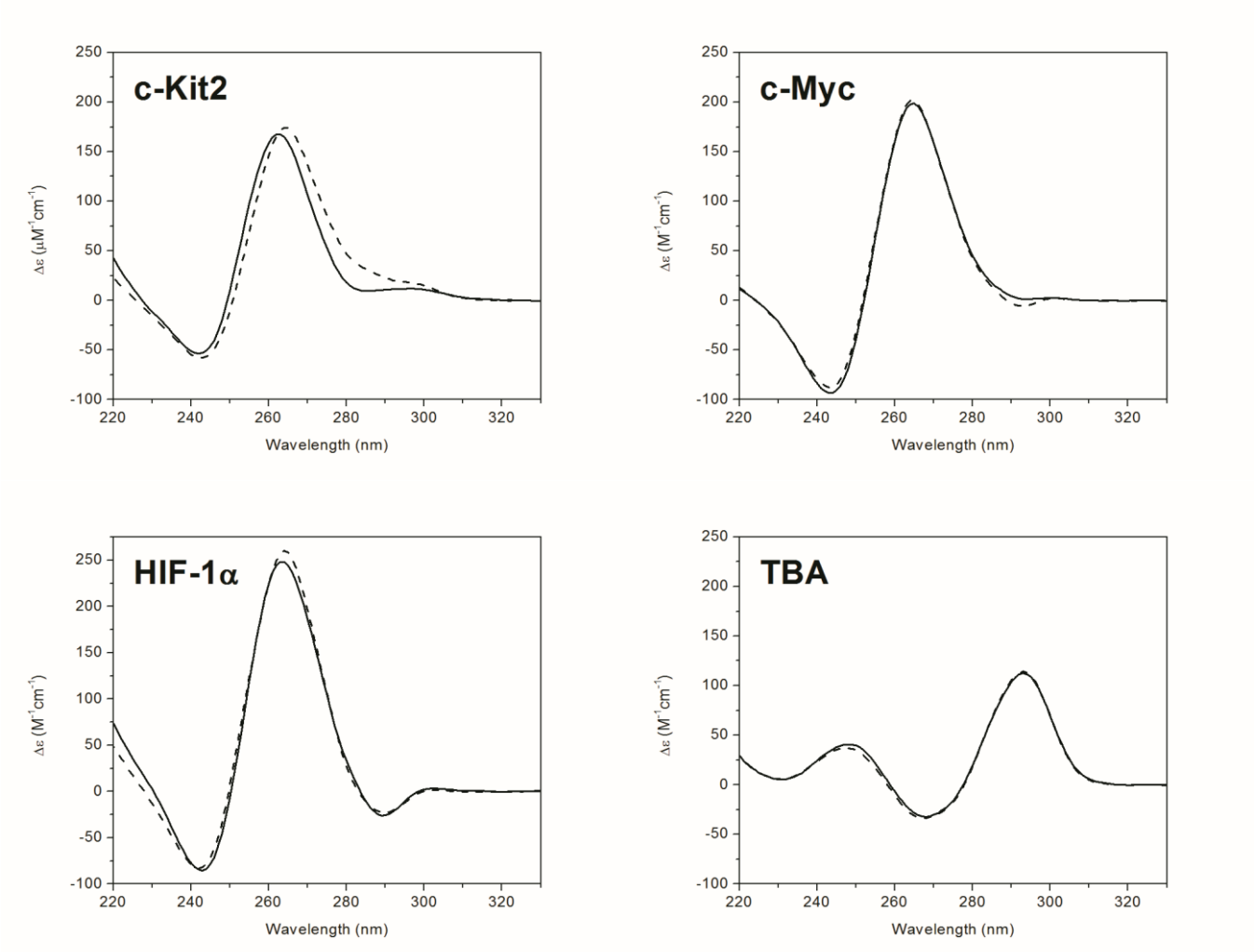

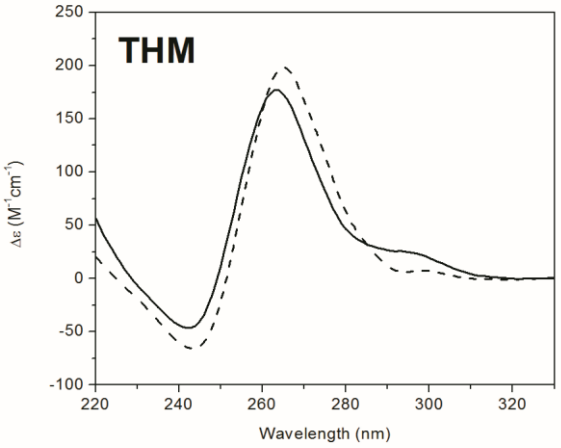
THM
Δε (M⁻¹cm⁻¹)
Wavelength (nm)

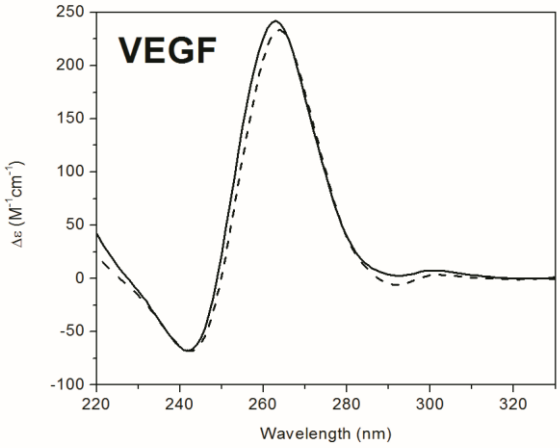
VEGF
Δε (M⁻¹cm⁻¹)
Wavelength (nm)

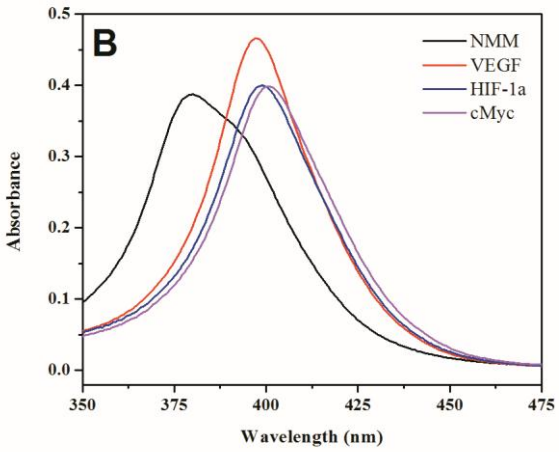
B
NMM
VEGF
HIF-1a
cMyc
Absorbance
Wavelength (nm)

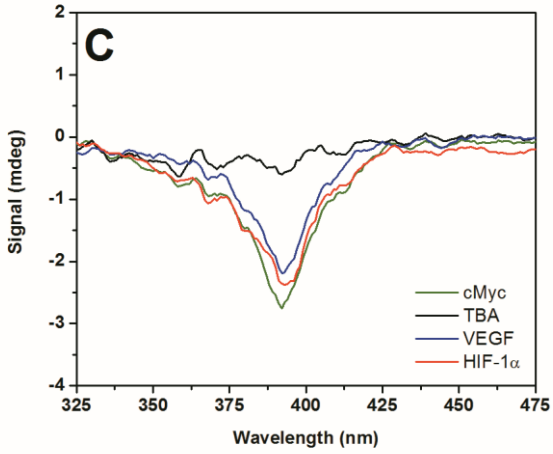
C
cMyc
TBA
VEGF
HIF-1α
Signal (mdeg)
Wavelength (nm)

Figure S5.

Figure S5. (**A**) Wavelength scans for equilibrium CD titration of 2.5 μM Tel22 in the presence of 2 equivalents of NMM annealed in 10 mM LiCac, pH 7.2 with KCl. Each sample was incubated for >30 h at 30°C after addition of indicated amount of KCl. (**B**) Normalized CD signal at 264 nm. Solid line represents the best fit of the data to Hill equation. (**C**) Control experiment. CD signature of Tel22 alone in a 10 mM lithium cacodylate buffer, pH 7.2, with increasing KCl concentration. All CD data were collected at 30 °C.

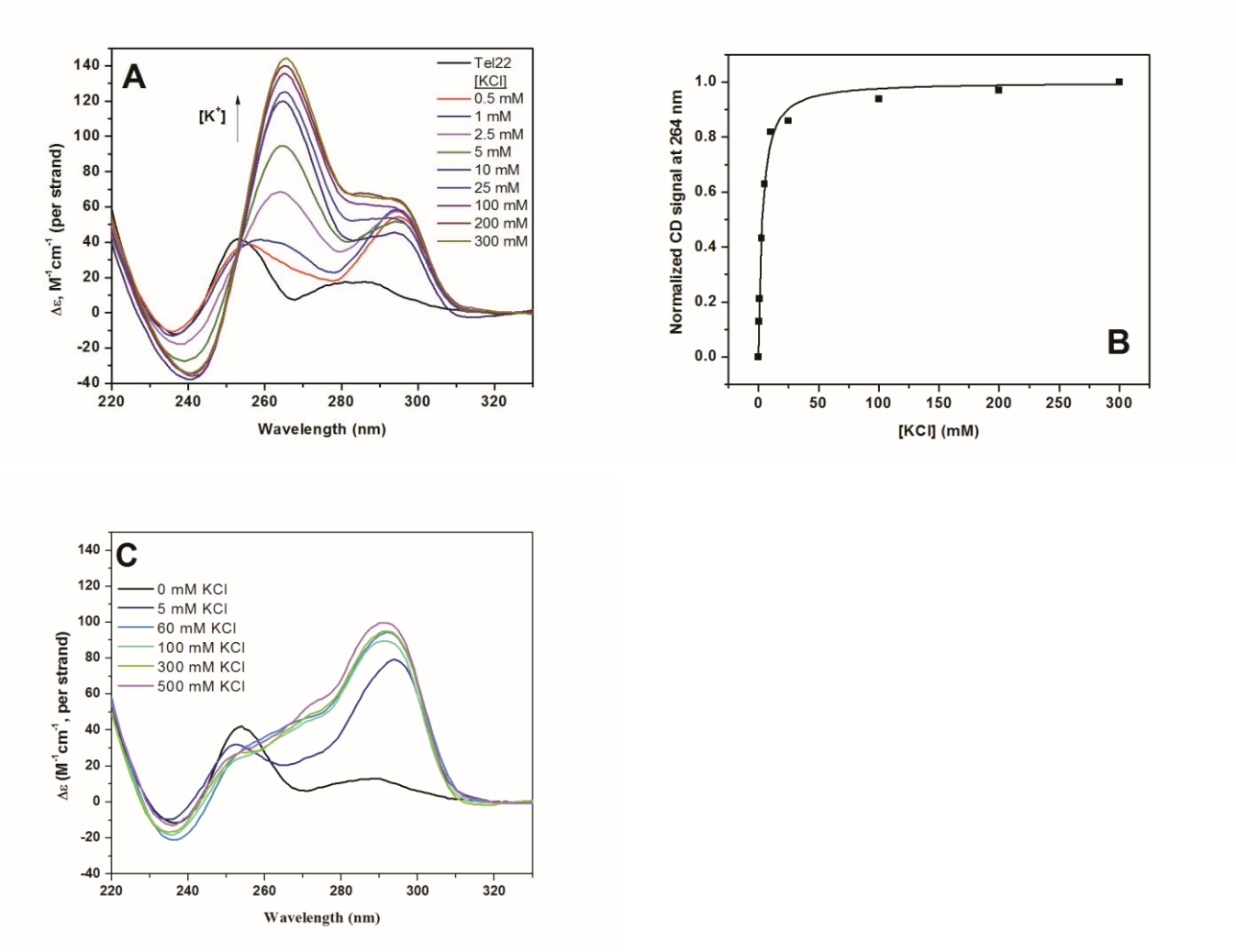

Figure S6.

Figure S6. Binding between NMM and Tel22 studied using UV-vis spectroscopy. (**A**) Nonequilibrium Job plot obtained from titrations of Tel22 into a solution of NMM (black squares) and from titration of NMM into a solution of Tel22 (solid red circles). (**B**) Equilibrium Job plot conducted using batch method. All data were collected at 25 °C in 5K buffer. In both cases data indicate 1:1 binding ratio between NMM and Tel22. *Continuous variation analysis* was used to obtain accurate values of stoichiometry for NMM binding to Tel22. NMM and Tel22 solutions of equal concentration were prepared in 5K buffer. Two sets of titrations were completed. First, 1.00 mL of 18 µM porphyrin solution was placed in two 1-cm cuvettes, one to be used as a reference. 25 – 100 µL aliquots of 18 µM GQ solution were added to the sample cell, while equal volume of buffer was added to the reference cell. Each sample was mixed thoroughly and incubated for 2 min before spectra collection. In the second set of titrations 1.00 mL of 18 µM Tel22 solution was placed in a sample compartment and 1.00 mM of buffer was placed in a reference cell. Both cells were titrated with 18 µM NMM solution. Difference spectra were collected in 350 – 700 nm range at 25 °C. Job plots were constructed by plotting the difference in the absorbance values at 376.0 and 402 nm versus mole fraction of NMM. The values of mole fraction at maxima or minima were used to obtain the stoichiometry of NMM binding to Tel22. In addition, equilibrium job plot experiments were performed using batch method. Twelve samples with various amounts of Tell 22 and NMM and constant total concentration of ~17 µM were prepared and incubated at 30 °C for >30 h before collecting UV-vis spectra. Data manipulation was done as described above.

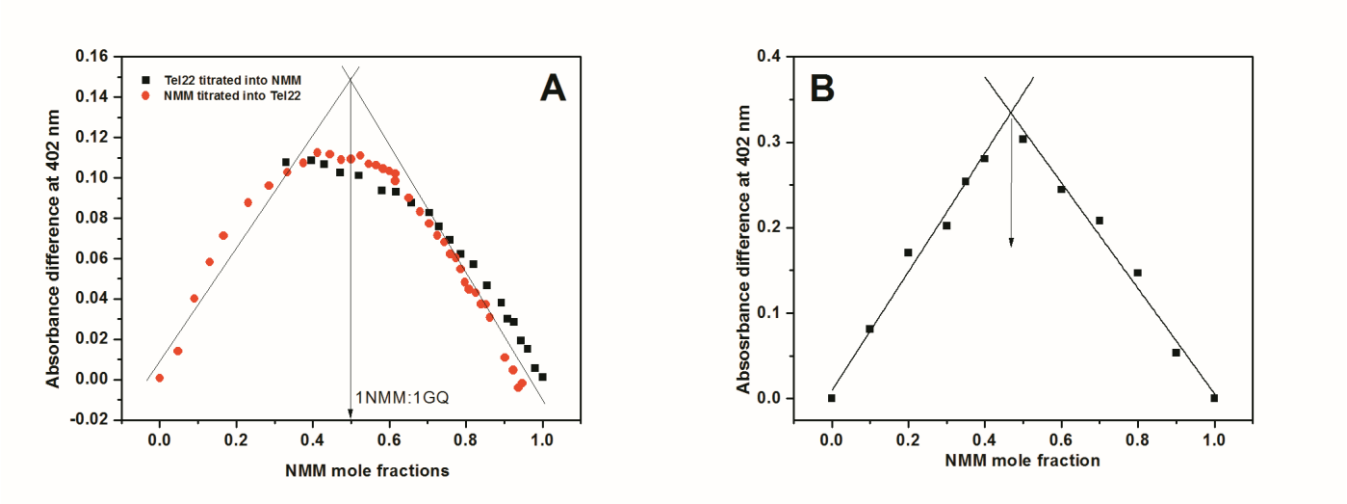

Figure S7

Figure S7. Visualization of gel shown in **Figure 5A** by NMM's fluorescence. Non-denaturing gel was prepared at 20 % acrylamide supplemented with 5 mM KCl. Tel22 strand concentration was 40 μM. (**A**) Gel visualized using UV-shadowing; (**B**) gel visualized using NMM's fluorescence (λ^{ex}=399 and λ^{em}=610 nm). Diffuse slow moving bands correspond to excess of free NMM. (**C**) CD spectra of the Tel22 samples to which NMM was added right before loading the gels (the last three lanes in part A). Note the similarity of these CD spectra to that of unaltered Tel22 in 5K buffer, consistent with PAGE gel results. There is a rather small increase in a peak at 264 nm indicating NMM-induced kinetically slow conversion of hybrid Tel22 to a parallel conformer.

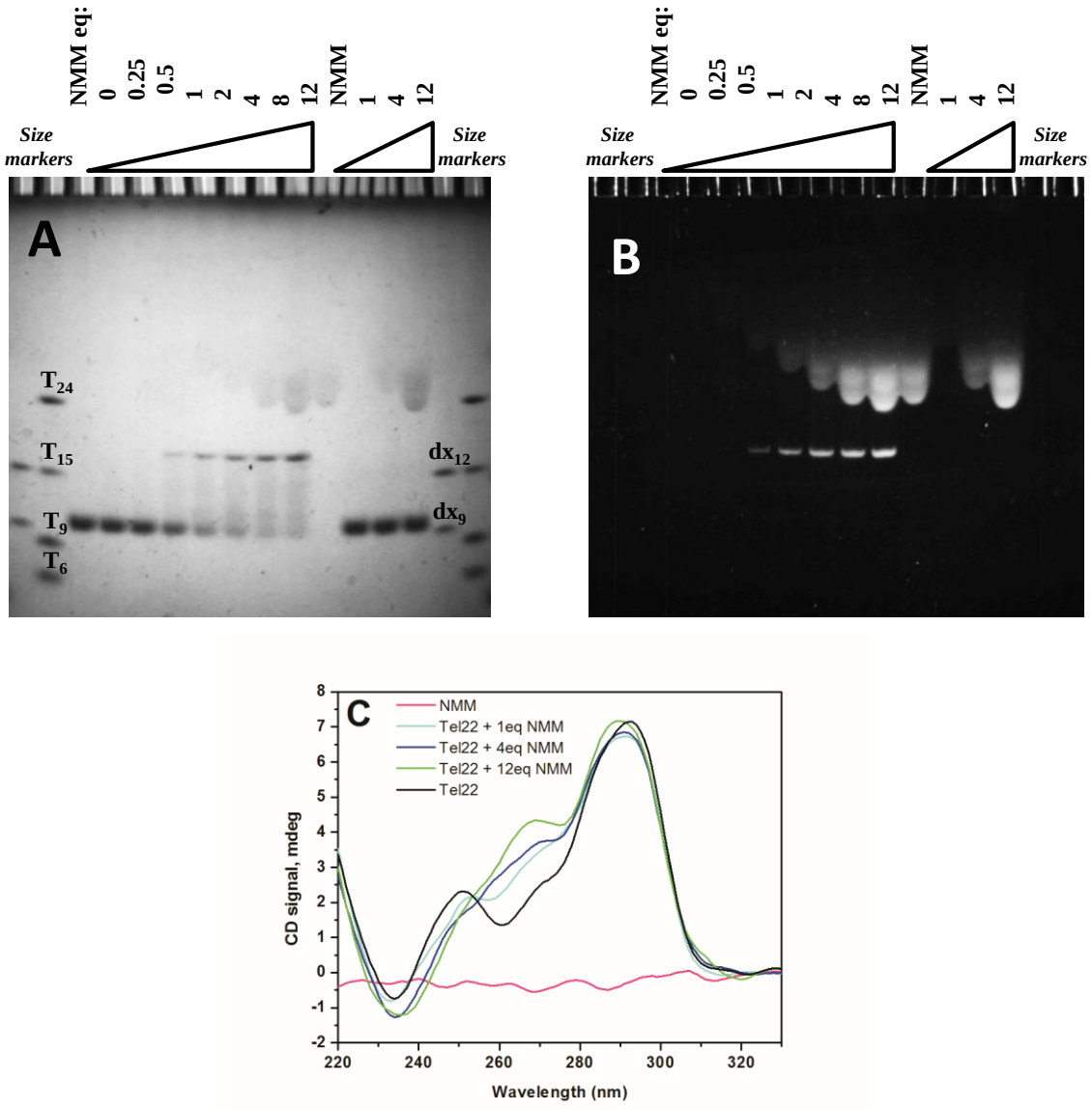

Figure S8

Figure S8. Strand mixing experiment. Samples of Tel22 were mixed with T_6Tel22 in 1:1 ratio and annealed with 2 and 8 equivalents of NMM. T_6Tel22 was chosen to have larger size but similar secondary structure to that of Tel22 and interact with NMM in a similar manner. (**A, B**) CD spectra of samples prepared for gels in (**C**). The gel samples were diluted right before collecting CD scans with 5K buffer to 2 μM. CD spectra were collected at 25 °C. Note the similarity of the CD signatures of Tel22 and T_6Tel22. (**C, D**) Non-denaturing gel was prepared at 20 % acrylamide supplemented with 5 mM KCl. DNA strand concentrations were 40 μM. (**A**) Gel visualized using UV-shadowing. (**B**) Gel visualized using NMM's fluorescence.

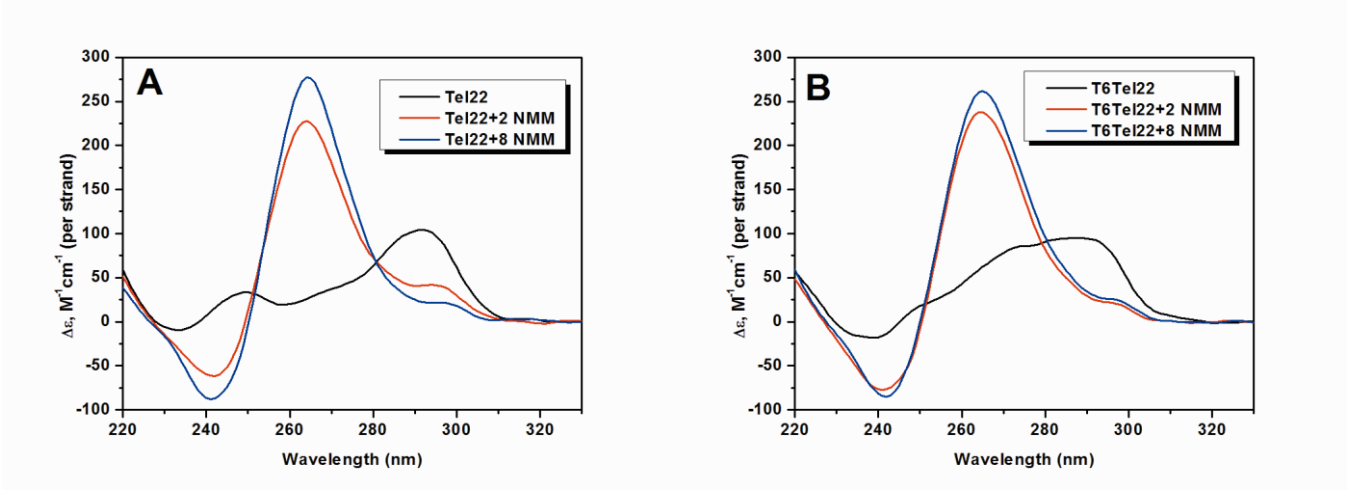

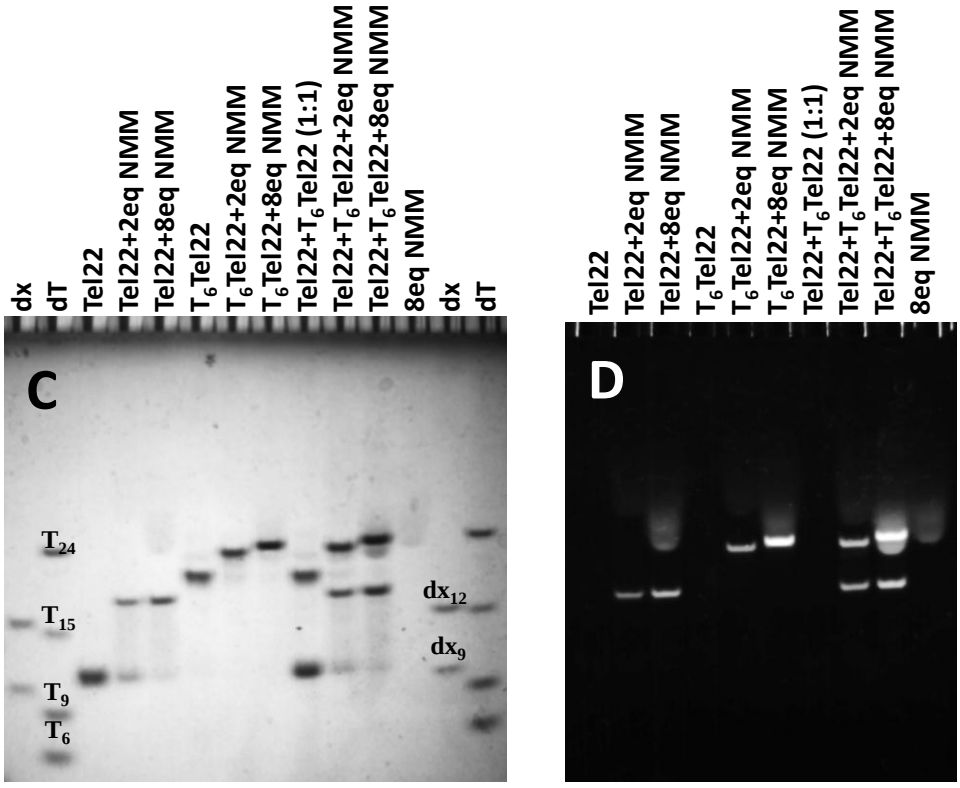

Figure S9

Figure S9. (**A**) 3D representation of equilibrium CD titration of Tel22 with NMM at 25 °C, where concentration of Tel22 is 40 μM. (**B**) Normalized singular values and fraction of total variance (RV) for first 8 components. (**C**) First-order autocorrelation values of U and V matrices for first 8 components. (**D**) CD basis spectra (U×S) for the two major components that constitute to equilibrium NMM-Tel22 mixture. (**E**) Comparison of CD spectra of component 2 of SVD and Tel22 in 50Na. Note, since intensities of component 2 are in arbitrary units, this spectrum was normalized to the 295 nm peak of Tel22 in 50Na for comparison. (**F**) Amplitude vectors V for the first two components.

The singular values (S), relative variance (RV) (**B**), autocorrelation values (**C**) as well as the scaled basis spectra (U×S) (**D**) indicate that only the first two components contribute to the spectra. Components 1 and 2 have characteristic signature of predominantly parallel and antiparallel GQ conformations, respectively. The superposition of component 2 with the CD signal of Tel22 annealed in 50Na buffer shows the similarity of the two spectra (**E**). The amplitude vectors (**F**) demonstrate that component 1 increases with the increased amount of added NMM in the expense of component 2, confirming that NMM-induced structural conversion is a loss in the antiparallel component of Tel22.

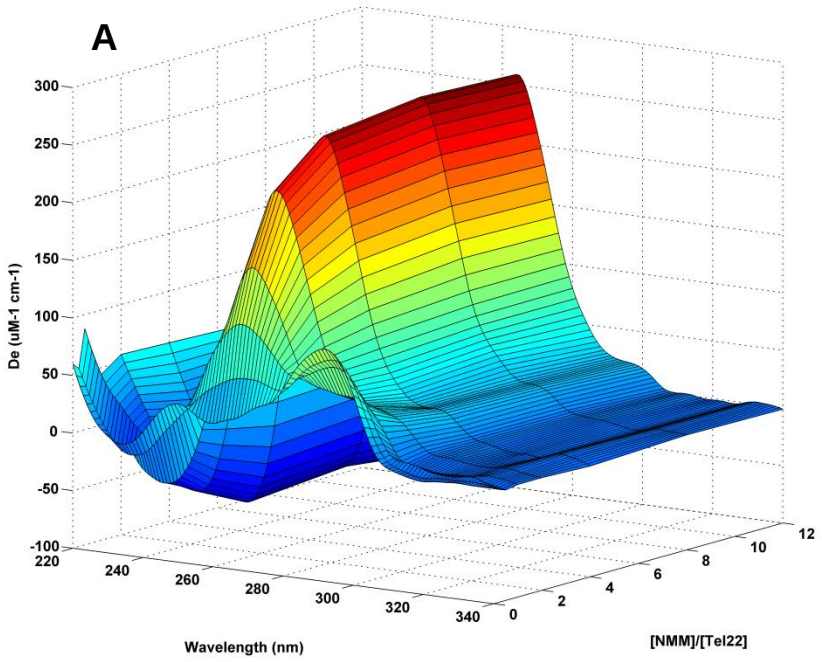

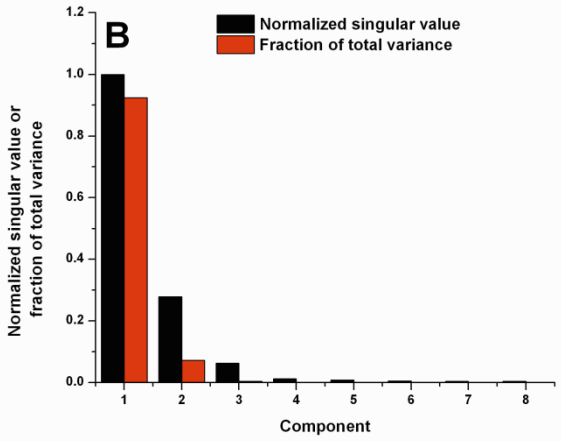
B
Normalized singular value
Fraction of total variance
Normalized singular value or fraction of total variance
Component

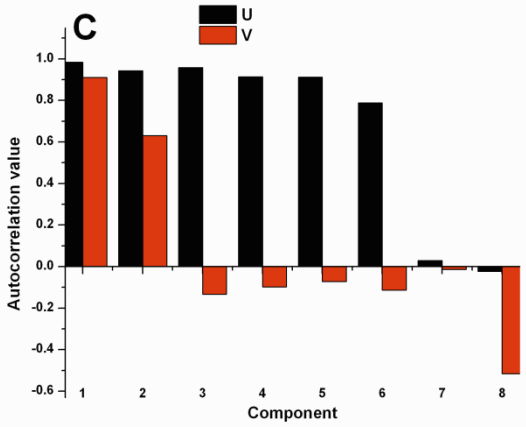
C
U
V
Autocorrelation value
Component

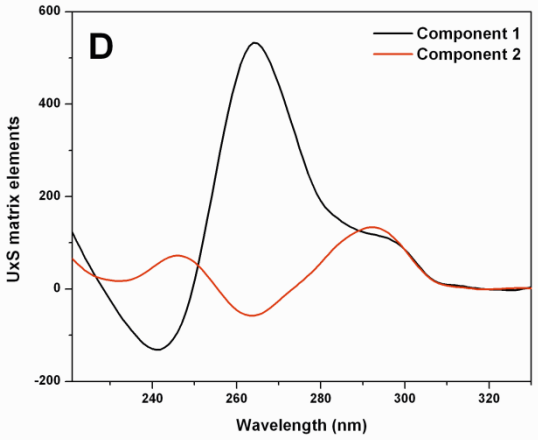
D
Component 1
Component 2
UxS matrix elements
Wavelength (nm)

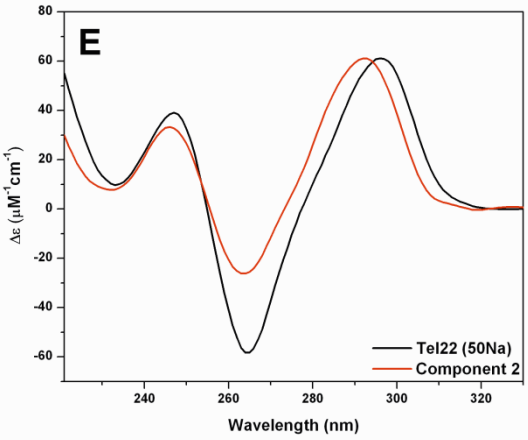
E
Tel22 (50Na)
Component 2
Δε (μM⁻¹cm⁻¹)
Wavelength (nm)

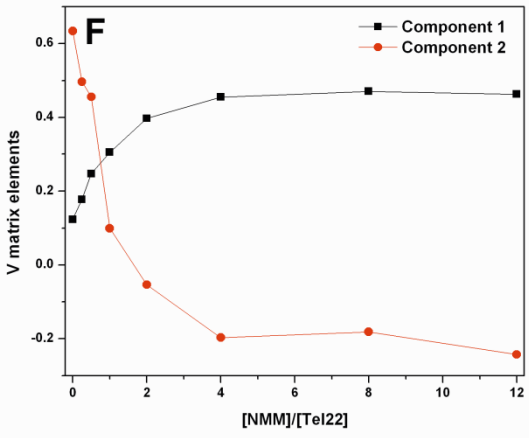
F
Component 1
Component 2
V matrix elements
[NMM]/[Tel22]

Figure S10

Figure S10. Gel electrophoresis experiments. Non-denaturing gel was prepared at 20 % acrylamide supplemented with either 10 mM NaCl (**A, B)** or 10 mM LiCl (**C, D)**. Tel22 strand concentration was 40 μM. Size markers (single stranded polythymidylate dT_6, dT_9, dT_{15}, dT_{24}) are provided. In the first 8 lanes, Tel22 samples were annealed with increasing amount NMM slowly cooled to 30 °C and incubated at 30 °C for >12 h. The next lane was loaded with 8 eq. of NMM without Tel22. In the last 3 lanes, 1, 4, and 12 eq. of NMM was added to annealed Tel22 right before loading gel. Gels were visualized using UV-shadowing (**A, C**) and NMM's fluorescence (**B, D**).

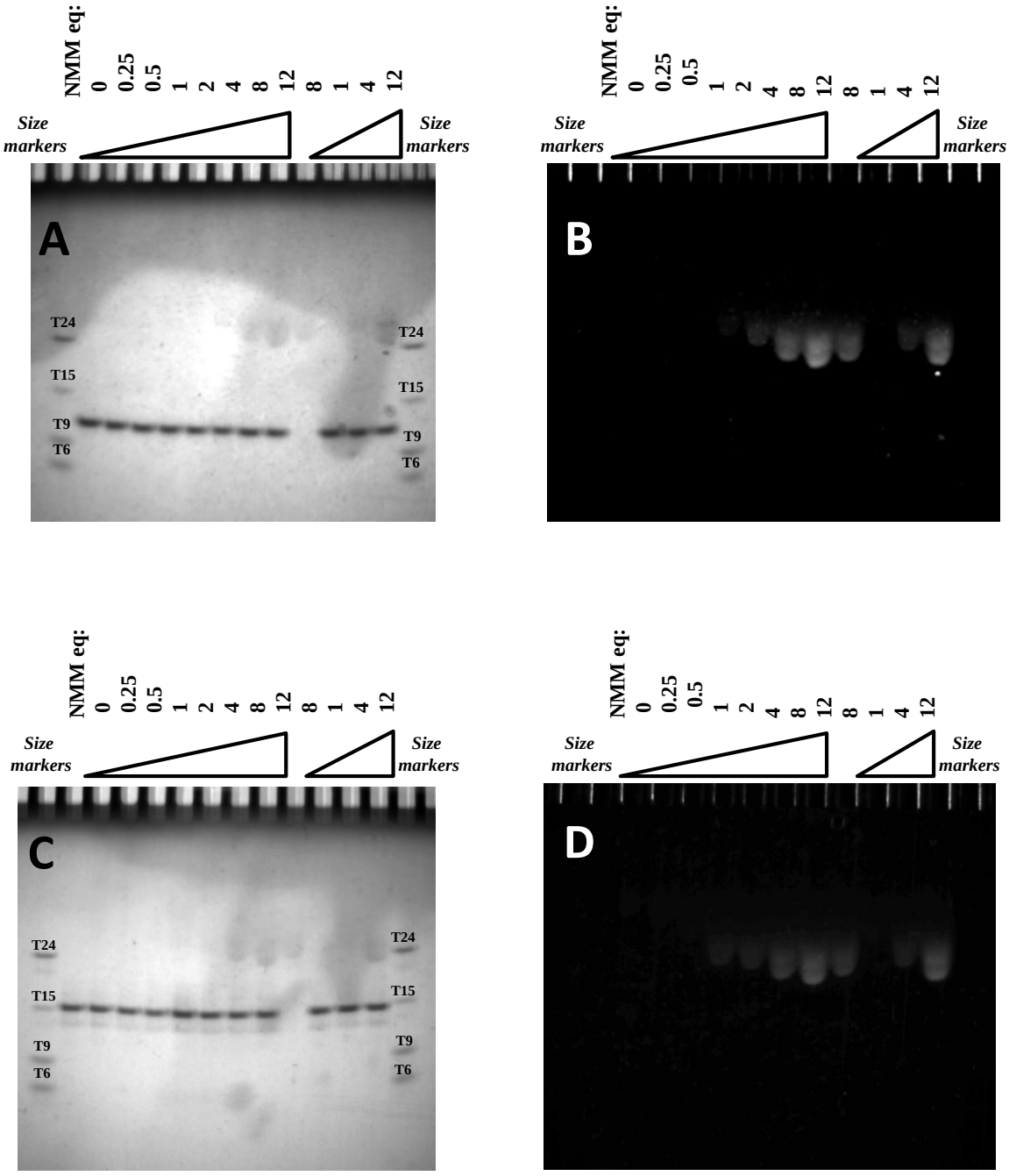

Figure S11

Figure S11. Characterization of fluorescently labeled oligonucleotides F21D in 5K and 50Na and FGD in 5K. (**A**) TDS spectra for F21D and FGD. TDS resulted from the difference between UV-vis spectra collected at 90.0 °C and at 25.0 °C. (**B**) CD spectra of F21D and FGD at 25 °C. Both CD and TDS spectra were recorded in the 1 mm pathlength quartz cuvette. Oligonucleotides were prepared at 10 μM concentration and annealed directly in the UV-vis instrument by heating at 90°C for 10 min, cooling to room temperature over 4 h and incubating overnight at 4°C. TDS and CD indicate unambiguously the quadruplex formation.

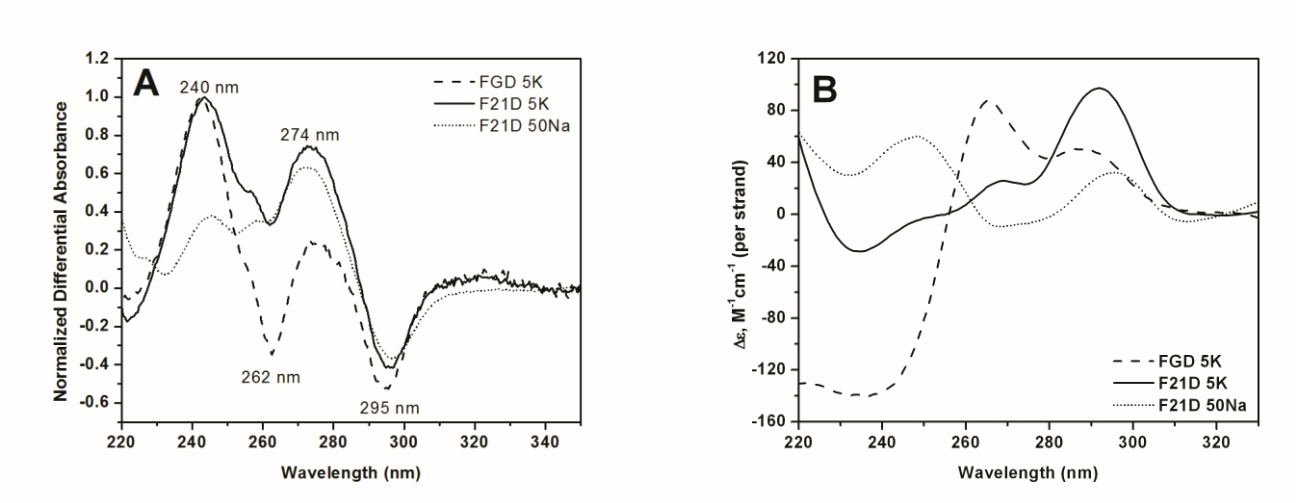

Figure S12

Figure S12. FRET melting of FGD in the presence of porphyrins and competitors. (**A**) Increase in the stabilization temperature, $\Delta T_{1/2}$, of 0.2 μM FGD as a function of porphyrin concentration. (**B**) Stabilization of FGD by NMM or NMP in the presence of duplex DNA competitors, ds26 or CT or (**C**) parallel stranded GQ competitors $[dTG_5T]_4$, G5, and $[dTG_8T]_4$, G8. Concentrations of porphyrins and FGD were fixed at 1.6 and 0.2 μM, respectively. Amount of competitor is indicated in the figure legend. All experiments were performed in 5K buffer.

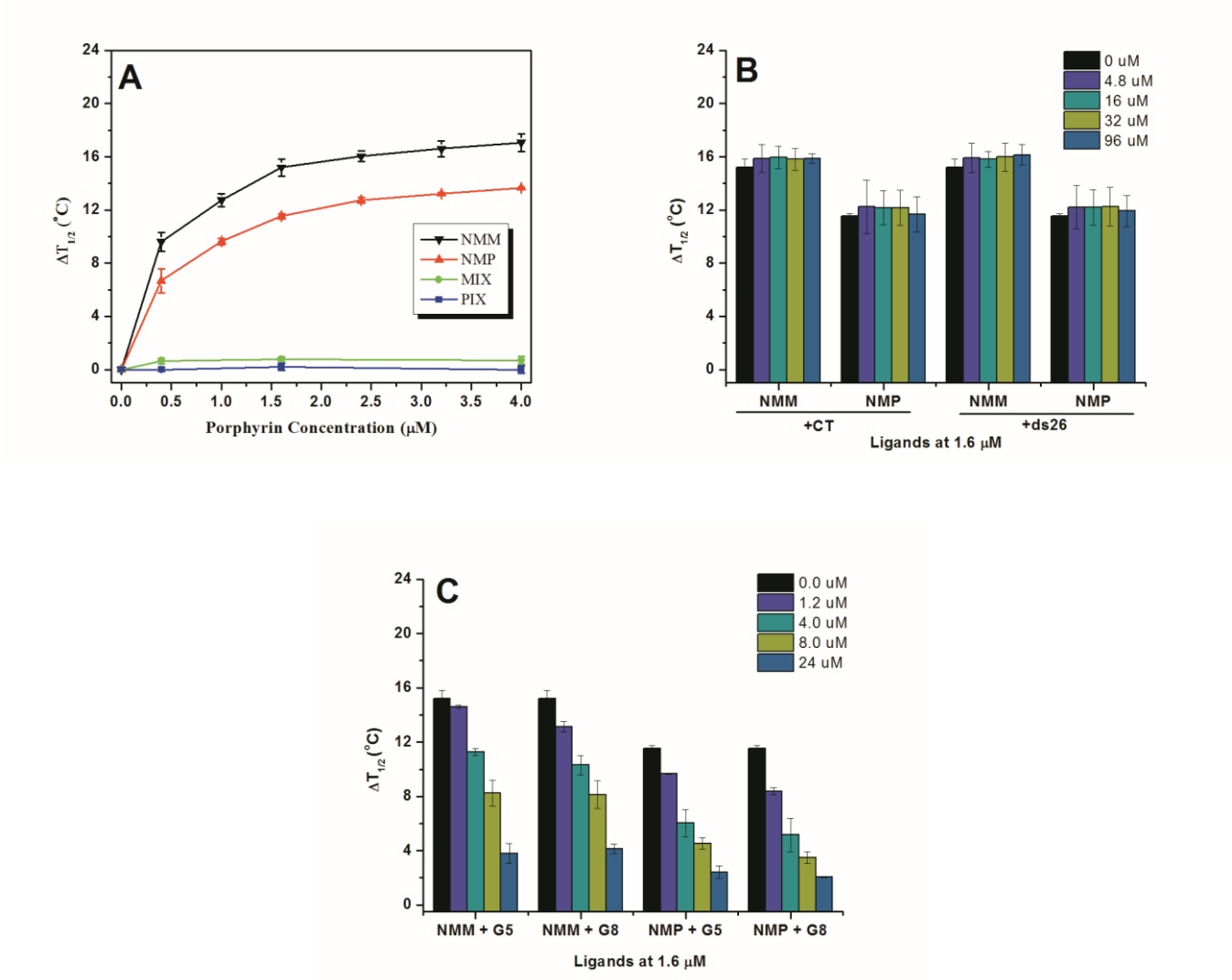

Figure S13

Figure S13. Stabilization of F21D in 50Na buffer by NMM and NMP in FRET melting assays. (**A**) Representative melting profiles for 0.2 μM F21D in the presence of increasing amounts of NMM. Melting of F21D alone is shown by black symbols. (**B)** Concentration dependence of stabilization temperature for 0.2 μM of F21D in the presence of NMM and NMP. Each experiment was repeated 2 times.

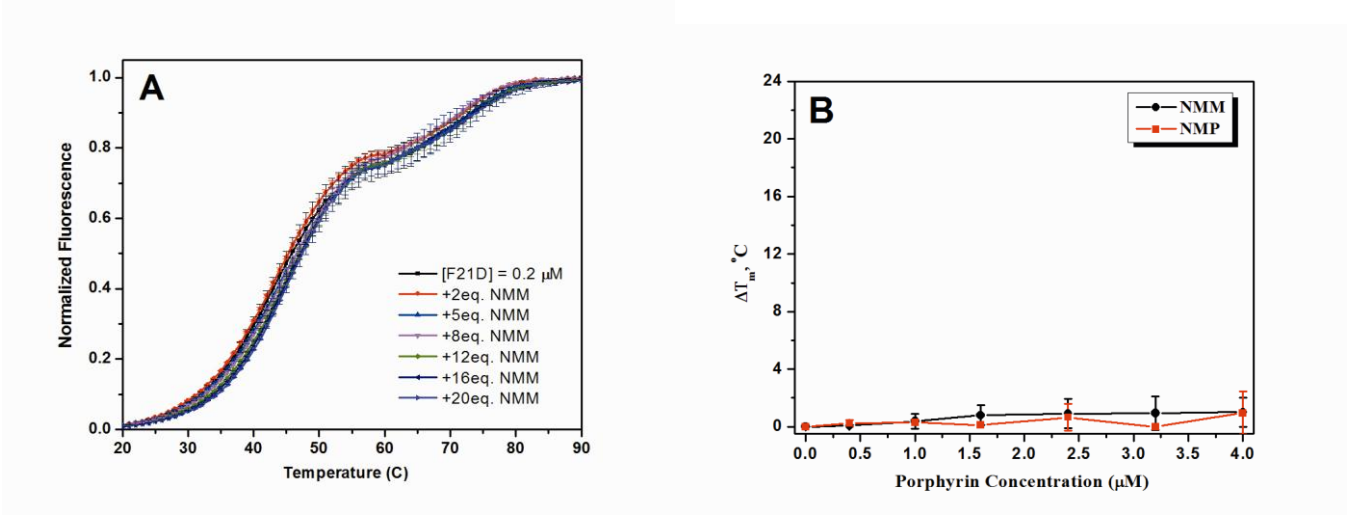

Figure S14

Figure S14. FRET melting of 0.2 μM F21D (or FGD) in the presence of 1.6 μM TMPyP4 and competitor duplex DNA, ds26 or CT, the amount of which is indicated in the figure legend. All experiments were performed in 5K buffer and repeated two times. Note, the melting temperature of F21D and FGD with 1.6 μM TMPyP4 and in the absence of any competitor was > 95 °C. Therefore the displayed $\Delta T_{1/2}$, in fact, represents the lower limit of the actual value.

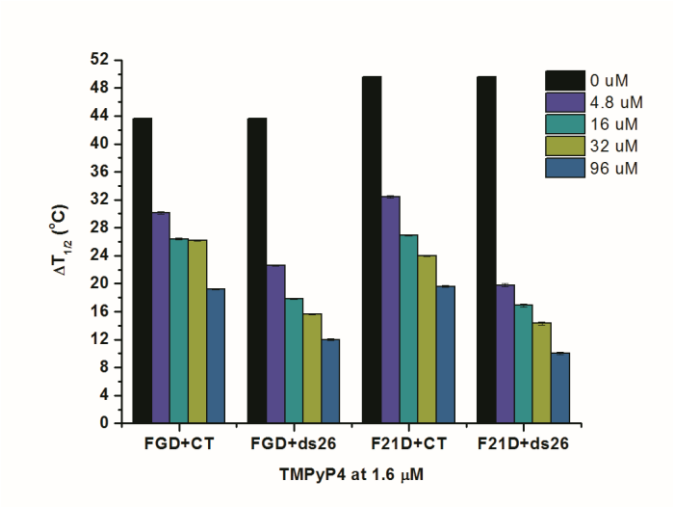

Figure S15

Figure S15. CD melting data for HIF-1α collected at 264 nm. HIF-1α was annealed in 5K buffer at ~4 μM with and without 2 equivalents of NMM and incubated at 30 °C for > 12 h. Melting data are represented by solid shapes (black squares for HIF-1α; grey triangles for HIF-1α+NMM) and cooling data are indicated by open shapes (squares for HIF-1α and triangles for HIF-1α+NMM). The inset shows the derivatives of the smoothed melting curves used to determine $T_{1/2}$ values. Arrows indicate the direction of temperature change. Note, starting equilibrated HIF-1α sample is a mixture of at least two GQs, kinetic and thermodynamic, with the latter being a major conformation. Upon heating, melting of both components is observed. When HIF-1α sample is cooled, only kinetic product is reformed on the time scale of this experiment. Situation changes when NMM is added to HIF-1α. This porphyrin shifts the equilibrium toward thermodynamic product both in melting and cooling profiles. NMM, therefore, accelerates thermodynamic product formation in HIF-1α.

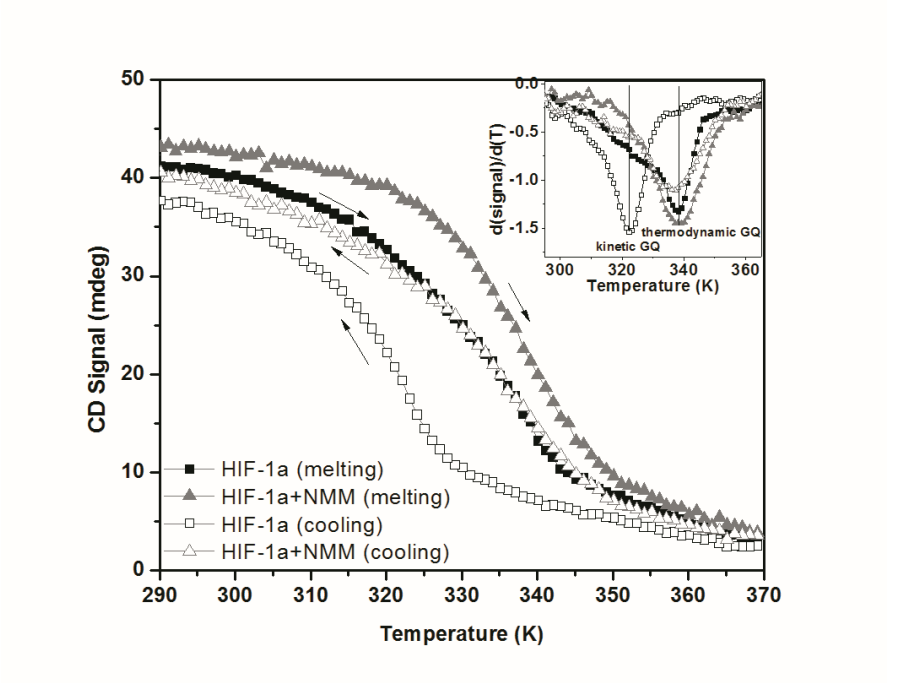

References

45. Ren, J. and Chaires, J.B. (1999) Sequence and structural selectivity of nucleic acid binding ligands. *Biochemistry*, **38**, 16067-16075.
53. Cantor, C.R., Warshaw, M.M. and Shapiro, H. (1970) Oligonucleotide interactions. 3. Circular dichroism studies of the conformation of deoxyoligonucleotides. *Biopolymers*, **9**, 1059-1077.
56. Gray, R.D. and Chaires, J.B. (2011), *Current Protocols in Nucleic Acid Chemistry*. John Wiley & Sons, Inc., pp. 17.14.11-17.14.16.
61. Gray, R.D. and Chaires, J.B. (2011) Linkage of cation binding and folding in human telomeric quadruplex DNA. *Biophysical Chemistry*, **159**, 205-209.
71. Pasternack, R.F., Gibbs, E.J. and Villafranca, J.J. (1983) Interactions of porphyrins with nucleic acids. *Biochemistry*, **22**, 2406-2414.
84. Haq, I., Chowdhry, B.Z. and Chaires, J.B. (1997) Singular value decomposition of 3-D DNA melting curves reveals complexity in the melting process. *European Biophysics Journal*, **26**, 419-426.
85. Henry, R.W. and Hofrichter, J. (1992) In Ludwig Brand and Johnson, M. L. (eds.), *Methods in Enzymology*. Academic Press, Vol. Volume 210, pp. 129-191.
86. Gray, R.D. and Chaires, J.B. (2008) Kinetics and mechanism of K^+- and Na^+-induced folding of models of human telomeric DNA into G-quadruplex structures. *Nucleic Acids Res.*, **26**, 4191-4203.
87. Scolaro, L.M., Castriciano, M., Romeo, A., Patane, S., Cefali, E. and Allegrini, M. (2002) Aggregation behavior of Protoporphyrin IX in aqueous solutions: clear evidence of vesicle formation. *J. Phys. Chem. B*, **106**, 2453-2459.